Anal Bioanal Chem (2010) 396:707–714
DOI 10.1007/s00216-009-3276-9

ORIGINAL PAPER

Magnetic-based purification system with simultaneous sample washing and concentration

Qasem Ramadan · Ting Ting Lau · Shihan Bryan Ho

Received: 25 August 2009 / Revised: 28 October 2009 / Accepted: 31 October 2009 / Published online: 18 November 2009

Abstract Simultaneous washing and concentration of magnetic microparticles was demonstrated using a rotational magnetic system under a continuous-flow condition. The rotation of periodically arranged permanent magnets close to a fluidic channel carrying a suspension of magnetic particles allows the trapping and releasing of particles along the fluidic channel in a periodic manner. Each trapping and releasing event resembles one washing cycle in conventional biological assays. Concentration efficiencies of 99.75±0.083% at a flow rate of 200 μl/min and 88.10±3.17% at a flow rate of 1,000 μl/min and a purification efficiency of 99.10±4.3% at a flow rate of 900 μl/min were achieved.

Keywords Continuous flow · Washing · Separation · Magnetic particles

Electronic supplementary material The online version of this article (doi:10.1007/s00216-009-3276-9) contains supplementary material, which is available to authorized users.

Q. Ramadan
Bioelectronics Program, Institute of Microelectronics,
11 Science Park Road,
Singapore 117685, Republic of Singapore

T. T. Lau
Nanyang Technological University,
Nanyang Avenue,
Singapore 639798, Republic of Singapore

S. B. Ho
Department of Biomedical Engineering,
National University of Singapore,
10 Kent Ridge Crescent,
Singapore 119260, Republic of Singapore

Present Address:
Q. Ramadan (✉)
Swiss Federal Institute of Technology (EPFL),
Laboratory of Microsystems,
1015 Lausanne, Switzerland
e-mail: qasem.alramadan@epfl.ch

Introduction

Functionalized nanoscale/microscale magnetic particles have proven to be an efficient tool for manipulating a wide variety of analytes, including viruses, proteins, DNA, RNA, cells, and bacteria. Therefore, the utilization of such particles has received increasing interest [1–3] since they can be coated with a selected ligand against the target of interest and they can be remotely manipulated thanks to their superparamagnetic nature. Furthermore, their large surface-to-volume ratio allows an efficient separation in microfluidic environments. In immunomagnetic assays, the magnetic particles are used as a solid-phase carrier for bioanalyzed targets to render them magnetic and to make them responsive to external magnetic fields. The magnetic particles are typically coated with a reagent which has a specific affinity for a target analyte. Subsequently, once the magnetic particles have been introduced into a solution, they will only attach to the target analyte. The magnetic particle–analyte complex is then separated from the solution using a magnet. Following this, the magnetic particle–analyte complex is washed in a buffer solution.

Conventional methods of washing magnetic particles [4] include pipetting buffer solution into a reaction vessel containing the sample to suspend the particles in the buffer solution and separating them using a magnet. This is followed by a suction step that separates the solid phase

from the liquid phase. During these suspension and suction steps, a washing cycle of the solid phase takes place and, if needed, these steps are repeated to carry out the required number of cycles till the analyte is of a suitable purity.

Several magnetic separation devices have demonstrated the separation of magnetic particles in a microfluidic channel utilizing an external permanent magnet [5–7], integrated magnetic posts [8, 9], or an integrated micro-electromagnet [10, 11]. However, these devices and/or processes still have a major drawback, which is the capture of the magnetic particles occurs only at the wall of channels/tubes in a static trapping mode. In practical applications, such as cell sorting, high magnetic particle concentrations are used and the magnetic fields usually create relatively large aggregates during the magnetic separation process owing to the significant dipole–dipole interactions [12]. The static trapping process results in inhomogeneous aggregates. In other words, not only the magnetic particle–analyte complex will be trapped, but other particulates (impurities) will also be physically trapped in the large aggregate created and in different concentrations depending on the homogeneity of the original raw sample.

In conventional assays, a relatively large single aggregate is formed against the sample container (tube) and the carrier fluid is aspirated by a pipette. Then the separated sample is suspended in a smaller volume of a new buffer and transferred afterward to downstream processes (detection). In recently reported devices, such as those described in the works cited above, the sample is washed by applying a washing buffer solution while the magnet is holding the magnetic particle–analyte complex. Such a washing step only removes impurities in the liquid surrounding the aggregate and other sandwiched impurities will stay trapped inside the aggregate. As such, it is necessary to carry out subsequent washing steps before the analyte can be analyzed further. However, in carrying out several subsequent washing steps, there is the risk that quantities of analyte may be lost during transfers between different washing containers, by evaporation and by adsorption to the wall of the containers. In the case of a low concentration of analyte in the starting sample (e.g., pathogens in drinking water and circulating tumor cells), carrying out the extraction and washing of the analyte using conventional methods may cause complete loss or a sharp decrease of the amount of analyte such that it may become undetectable.

In this paper we report a miniaturized and continuous-flow magnetic separation system (MSS) for sample concentration and purification in a closed-loop protocol that minimizes human interference, sample loss, and cross-contamination.

Theory

The concept of the present approach is based on an "alternate trapping and releasing" mechanism under continuous-flow conditions. The mechanism is shown schematically in Fig. 1. The drawing shows a fluidic channel through which a magnetic particle suspension is flowing with a low Reynolds number and a permanent magnet is positioned beneath the channel. The magnet rotates continuously around its short axis. The rotational motion of the magnet modifies the interaction between the magnetic particle suspension and the magnet in a periodic manner as illustrated in Fig. 1. Therefore, a dynamic and time-dependent interaction takes place between the mag-

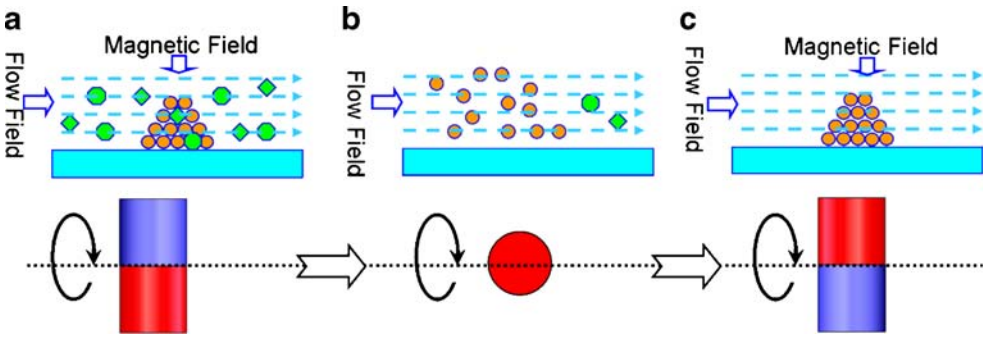

Fig. 1 The alternate trapping and releasing of a magnetic particle suspension by magnet rotation. The magnetic force changes during the magnet rotation from a maximum to a minimum then back to a maximum, etc. Magnetic particles are trapped in the channel when the magnetic force is a maximum and are released when the magnetic force is a minimum. *a* both magnetic and flow fields are on and therefore magnetic particles cluster and nonmagnetic particles keep flowing downstream. But some nonmagnetic particles can be physically trapped in the clusters. *b* the magnetic field is off or weak and therefore magnetic particle clusters disperse in the fluid and flow downstream and nonmagnetic particles are released and flow downstream with velocity higher than that of the magnetic ones. *c* purified magnetic particle cluster

net and the magnetic particle suspension, as explained in Table 1.

The magnetic particle suspension will be exposed to a strong magnetic field when the magnet's pole (north or south) points at the channel, i.e., $\varphi=0°$ (Fig. 1, step a), where φ is the angle between the normal of the magnet pole and the normal of the channel surface. Therefore, particles are attracted and trapped in a steep magnetic potential well and form a cluster there. As the magnet rotates, the magnetic force on a magnetic particle will be modulated accordingly. The force sharply decreases when the magnet's pole becomes out of phase with the channel, i.e., $0°<\varphi<90°$, until it becomes a minimum when the magnet's pole becomes perpendicular to the channel surface, i.e., $\varphi=90°$ (Fig. 1, step b) and hence the magnetic particles demagnetize, disperse, and flow with the carrier fluid. The magnetic force drops to its minimum value when the magnet rotates 90° around its short axis. When the magnet continues to rotate, the magnetic force modulation will be reversed, i.e., from a weak force when $\varphi=90º$, it increases slightly when $90°<\varphi<180°$ to a maximum when $\varphi=180°$ (Fig. 1, step c). The continuous rotation of the magnet with frequency f (where f is the number of rotations per second) results in a continuous trapping and releasing of magnetic particles accordingly with the same frequency.

The rotating magnets always receive a new bolus of magnetic particle suspension from upstream. When a single rotating magnet is present beneath the fluidic channel, a single trapping and releasing cycle and consequently one washing cycle occur. Such a washing cycle can be repeated for N cycles by using an array of rotating magnets arranged along the fluidic channel with the adjacent magnets having a separation S and a phase angle $\varphi=90°$ between them as illustrated in Fig. 2. The array of magnets rotates around one common axis, which is parallel to the fluidic channel, with a rotation frequency that can be adjusted according to the flow rate. When the magnetic particles are released from the first (now damped) potential well, they move with the carrier fluid toward the next growing potential well in a dispersed manner and during this translation time (T) the washing effect takes place. The translation time allows the particles to be detached from each other and spread out and consequently allows the release of any impurity that may have been trapped during a previous trapping event.

The simulated magnetic flux density and the simulated force due to three magnets arranged with orientation angles of $\varphi=0°$, $\varphi=90°$, and $\varphi=0°$ are shown in Fig. 3. The peaks show the locations where the magnet pole points at the channel and magnetic particles are subjected to a strong magnetic force (F_{mag}) and the flat portion of the curves shows the location where the pole is pointing away from the channel and the magnetic force is not strong enough to trap the particles; hence, particles are released.

The magnetic force required to trap a particle of volume V is given by $F_{\mathrm{mag}}=\frac{V\chi}{2\mu_0}\nabla\mathbf{B}^2$, where χ is the magnetic susceptibility of the particle, μ_{o} is the permeability of space, and $\boldsymbol{B}$ is the magnetic flux density produced by the magnet. In addition to the magnetic force, a magnetic particle of radius R experiences mainly a hydrodynamic drag force: $F_{\mathrm{d}}=6\pi\eta R\left(v_{\mathrm{p}}-v_{\mathrm{medium}}\right)$, where η, ν_{p}, and ν_{medium} are the medium viscosity, particle velocity, and medium velocity, respectively. Under conditions typical for the trapping of a magnetic bead, $\eta\cong10^{-3}\,\mathrm{N\,s\,m^{-2}}$, $R=10^{-6}\,\mathrm{m}$, and $v\approx10^{-6}\,\mathrm{m\,s^{-1}}$, this results in a drag force $F_{\mathrm{h}}\approx1.88\times10^{-12}N$.

Each cycle of trapping and releasing of particles represents a washing event similar to the washing process of biological samples using a microtiter plate. The trapping and releasing for N cycles allow N washing events to be run for the same bolus of magnetic suspension, which ensures an acceptable level of sample purity. At the end of the purification channel, the purified sample can now be collected and separated (Fig. 2) using a stationary strong magnet for downstream processing or detection.

Magnetic particle transport using such a mechanism has been reported with microscale devices [13, 14]. However, to achieve high trapping efficiency even in large channels using a permanent magnet (e.g., a NdFeB magnet) is a more efficient and straightforward task. The magnetic field generated by a permanent magnet can be on the order of 0.1 T compared with that generated by a planar microcoil ,which is in the range 1–10 mT. Macro-scale electromagnets can be customized to generate the required magnetic field, but the resultant electromagnet would be larger than a permanent magnet having the same

Table 1 Interaction of the magnetic particles with the magnet

Time (event)	φ	Magnetic force	Particle suspension status
t_1 (Fig. 1, step a)	0°	Maximum	Trapped in a cluster
t_2	$0°<\varphi<90$	Weak	Partially released
t_3 (Fig. 1, step b)	90°	Minimum	Released
t_2	$90°<\varphi<180°$	Weak	Partially trapped (start of trapping)
t_4 (Fig. 1, step c)	180°	Maximum	Trapped in a cluster

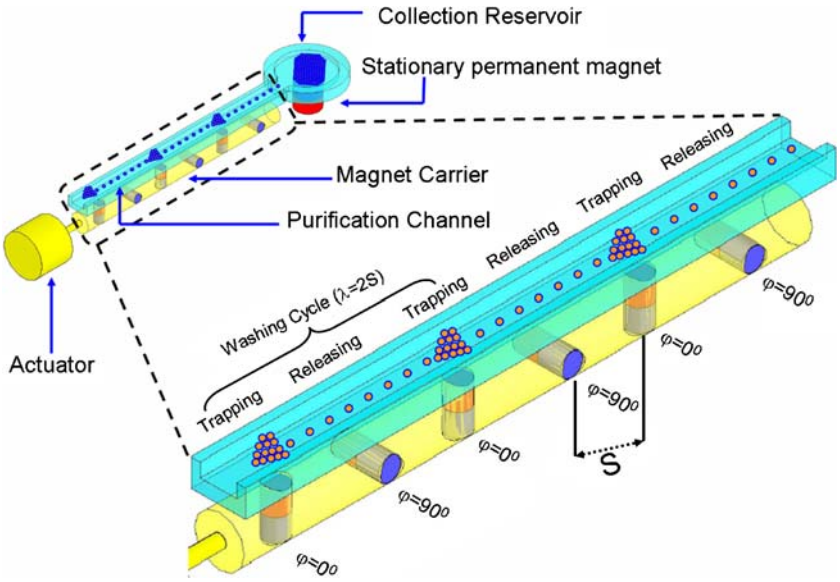

Fig. 2 The magnet array system. Magnetic particles are trapped in the channel when $\varphi = 0°$ and are released when $\varphi = 90°$ in periodic manner with cycle length (wavelength) $\lambda = 2S$, where S is the separation. The magnet array is rotated by employing a motor. *N* permanent magnets perform *N* washing cycles through a fluidic channel. The continuous and periodic trapping and releasing of the magnetic particles through the channel creates a path phase shift between the magnetic and nonmagnetic particles. Finally, the purified sample is collected in the collection reservoir using a stationary permanent magnet

magnetic field. Hatch and Stelter [15] reviewed the magnetic device design considerations for magnetic separation applications. Furthermore, electromagnets are prone to generate Joule heating, which may lead to sample heating and evaporation and may harm the bioorganism within the fluidic sample.

Experimental

A detailed description of the system's design and fabrication is provided as electronic supplementary material.

To measure the concentration and purification efficiencies of the MSS, sample turbidity and particle counting

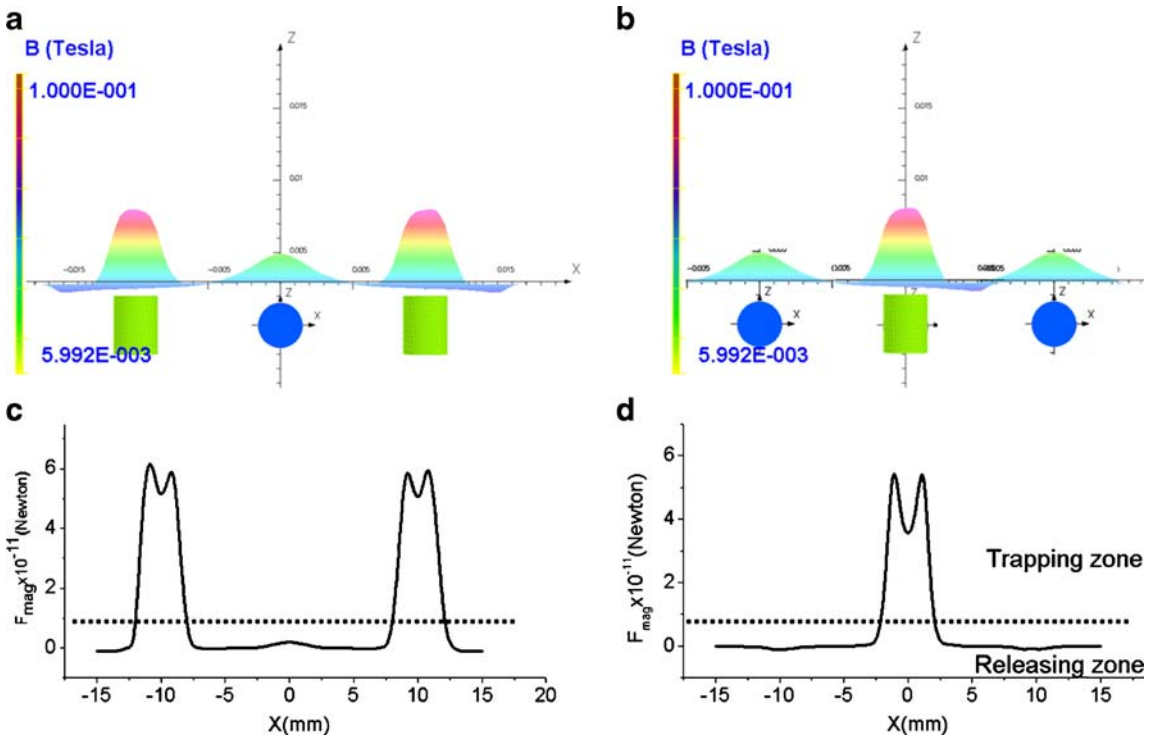

Fig. 3 Simulated magnetic flux density (**a**, **b**) and force (**c**, **d**) for three magnets each with 90° orientation to the previous/next one. The magnet with an orientation of 0° generates a magnetic force within the range of force required to trap the magnetic particles inside the channel, whereas the magnet with an orientation of 90° generates a very weak magnetic force that is not sufficient to trap the particles. The particle size was 1 μm and the separation between the magnet pole and the channel was 1.5 mm

methods were used. For this purpose, four solutions (particle suspensions) were used:

1. B1: A suspension of 0.97-μm-diameter magnetic particles (Estapor®) with a concentration of approximately 10^8 particles/ml in 10 ml of deionized water
2. B2: A suspension of 10-μm-diameter magnetic particles (Polysciences) with a concentration of approximately 10^5 beads/ml in 10 ml of deionized water
3. B3: A suspension of 6-μm-diameter silica particles (Polysciences) with a concentration of approximately 10^5 beads/ml in 10 ml of deionized water
4. B4: A 1:1 mixture of solutions B2 and B3

The concentration efficiency was measured by passing solution B1 through the MSS and collecting the waste at the channel outlet. To quantify the concentration efficiency, the turbidity (relative absorbance) of the waste samples was measured against that of the control sample (taken from the sample prior to passing it through the magnetic system) using a spectrophotometer. Then the concentration efficiency was calculated as $\mathrm{CE} = \left(1 - \frac{\mathrm{Q2}}{\mathrm{Q1}}\right) \times 100\%$, where CE is the concentration efficiency, Q1 is the original magnetic particle concentration in the sample before the injection into the system, and Q2 is the magnetic particle concentration in the waste solution.

The purification efficiency was measured by passing solution B4 through the MSS and collecting the waste sample at the channel outlet. With use of a hemocytometer, the concentration of nonmagnetic particles in the sample both before injection into the MSS and after passing them through it was calculated by counting the nonmagnetic particles at both ends. Then the sample was mixed thoroughly and six drops, each with a volume of 10 μm, were taken and spread over the hemocytometer and counted under a microscope using an objective magnification of ×50. Particle loss inside the channel owing to effects other than the magnetic force was quantified independently by passing the sample through the fluidic channel, which was mounted on a flat surface outside the MSS. The purification efficiency was calculated as $\mathrm{PE} = \left(1 - \frac{\mathrm{Q2}' - q}{\mathrm{Q1}'}\right) \times 100\%$, where PE is the purification efficiency, Q1′ is the number of the nonmagnetic particles in the sample before the injection into the MSS, Q2′ is the number of nonmagnetic particles in the waste sample, and q is the number of particles lost in the channel during the sample flow (this was measured independently).

The operation procedure of the purification system can be understood with reference to Fig. 4 by the following sequential steps:

1. Sample mixture (solution B4) was loaded into a syringe (syringe 1, 20 ml), fixed on a syringe pump and connected to the first inlet of the fluidic channel, which is mounted on the MSS, via Tygon tubing.

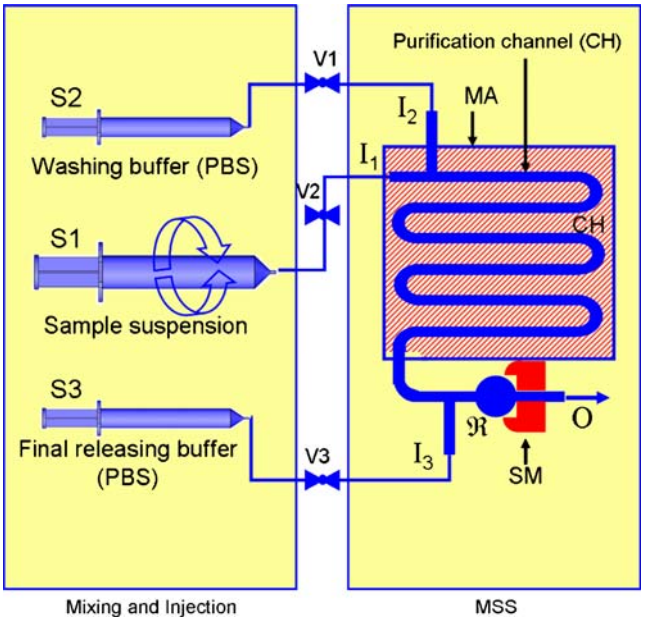

Fig. 4 Top view of the experimental setup (see the text for the detailed sequence of the sample concentration and purification). *S1* syringe 1, *S2* syringe 2, *S3* syringe 3, *PBS* phosphate-buffered saline, *V1* valve 1, *V2*, valve 2, *V3* valve 3, I_1 inlet 1, I_2 inlet 2, I_3 inlet 3, *MA* magnetic assembly, $\mathfrak{R}$ final collection reservoir, *SM* separation magnet, *O* outlet, *MSS* magnetic separation system

2. Two syringes (syringes 2 and 3) with buffer solution (phosphate-buffered saline) were mounted on two independently controlled syringe pumps. Syringe 2 was connected to the second inlet and syringe 3 was connected to the third inlet of the channel, which is located before the final collection reservoir. The fluid from syringes 1, 2, and 3 was controlled by three corresponding external valves, valves 1, 2, and 3, respectively.
3. The channel was firstly washed with a buffer solution from syringe 1 to push the air inside the channel: valve 1 is open and valves 2 and 3 are closed.
4. The MSS was switched on with both the magnetic assembly and the separation magnet positioned beneath the channel.
5. The sample (solution B4) was allowed to diffuse into the channel at a selected flow rate. The purification and separation started: valve 1 is closed, valve 2 is open, and valve 3 is closed.
6. When the sample had completely passed through, the magnetic assembly (see the electronic supplementary material) was pulled out so that the channel was free from the magnetic force of the magnetic assembly.
7. The channel was flushed again with the buffer solution from syringe 1 to remove residual particles that may stick to the channel wall: valve 1 is open, valve 2 is closed, and valve 3 is closed.

8. The separation magnet (see the electronic supplementary material) was pulled out and the purified and concentrated sample was flushed away from the channel by the buffer solution from syringe 3. One milliliter of phosphate-buffered saline was allowed to flow from syringe 3 with a relatively high flow rate (500 µl/min). Finally, the sample was collected in a small tube with a capacity of 1.5 ml through the channel outlet: valve 1 is closed, valve 2 is closed, and valve 3 is open.
9. Finally, the particle concentration of the sample collected was measured either by measuring the turbidity or by direct counting.

To investigate the effect of the number of washing cycles on the purification efficiency, a set of experiments were conducted by varying the number of magnet carriers by inserting one, two, or three magnet carriers or by reinjecting the sample into the MSS for a second time.

Sample homogeneity was maintained by continuously rotating the syringe during the injection. A custom-made rotating-syringe setup was integrated with a syringe pump which allows a semicircular (clockwise and counterclockwise) rotational movement of the syringe around its long axis. Such a mechanism ensured the administration of a homogeneous sample over the course of the experiment.

Results and discussion

Figure 5 shows the magnetic particle trapping in a fluidic channel mounted on top of the MSS. For the purpose of clear visualization, a high concentration of a suspension of iron oxide particles with an average diameter of 10 µm was used. Figure 5a show the magnetic particle suspension passed through a meandering channel on top of a stationary magnetic assembly, i.e., the magnet carriers are not rotated. Therefore, the particles continuously accumulated and clustered at all the magnets pointing to the channel surface. In this configuration, there is no trapping and releasing effect, but small particle clusters are formed. The small aggregation profile reduces the chance of impurity trapping by particle separation using the effect of magnetic field flow fractionation [16]. Figure 5b shows the results when the fluidic channel was introduced into the MSS and the magnetic particle suspension was passed through the channel while the magnets within the magnetic assembly were rotating with a frequency of 1/10. The series of images shows the particle trapping and releasing effect in one partition of the channel with only four trapping/releasing zones as shown at magnets A, B, C, and D. When the rotation angle $\varphi=0°$, magnets A and

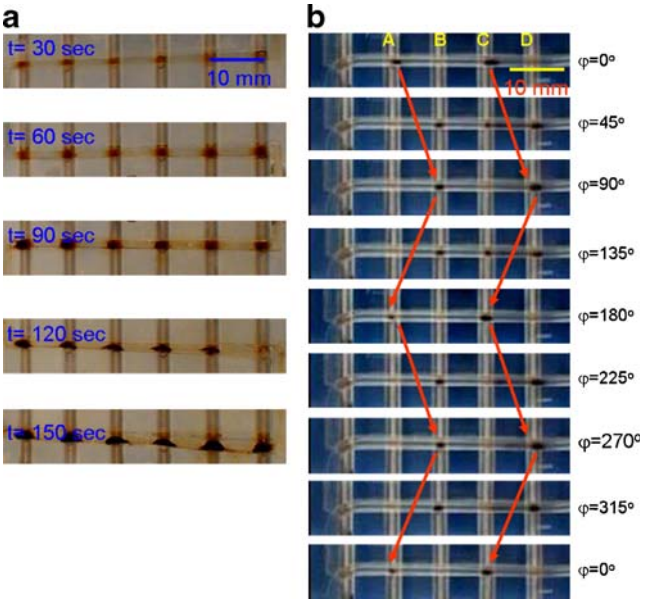

Fig. 5 **a** Trapping profile of magnetic particles with the stationary MSS. The particles accumulated in small clusters at all the trapping zones created by the active magnets. **b** Magnetic trapping profile with the rotating MSS. The magnetic particles move along the channel with a periodic trapping and releasing effect

C are active and hence particles are trapped at the corresponding trapping zones. When the magnet carriers rotated with an angle of $\varphi=45°$, particles were affected by a decreasing magnetic force and a filament of magnetic particles was created between magnets A and B and magnets C and D and then the particles were trapped at the zones corresponding to magnets B and D when $\varphi=90°$. At the rotation angle $\varphi=135°$, the magnetic forces at magnets B and D decreased and the particles started to escape the zones corresponding to magnets B and D and moved to the next trapping zones. Meanwhile magnets A and C received a new bolus of sample from the injection unit and the cycle was repeated in the same manner until all the particles were trapped in the last trapping zone by the separation magnet. The transition event of magnetic particles between each pair of adjacent magnets is a crucial event in the washing process through which the particles are dispersed to release unwanted particles from clusters.

The concentration efficiency was measured against the flow rate over the range 200–2,000 µl/min, as shown in Fig. 6. The concentration efficiency was in the range 87–99% for a flow rate of 200–1,000 µl/min and dropped when the flow rate was increased owing to the increase in the hydrodynamic force (increase of the particle velocity). The larger the particle size, the higher the magnetic force felt by the particle and consequently the higher the concentration efficiency. Therefore, when small magnetic particles (e.g., nanoscale) are used, the magnetic assembly

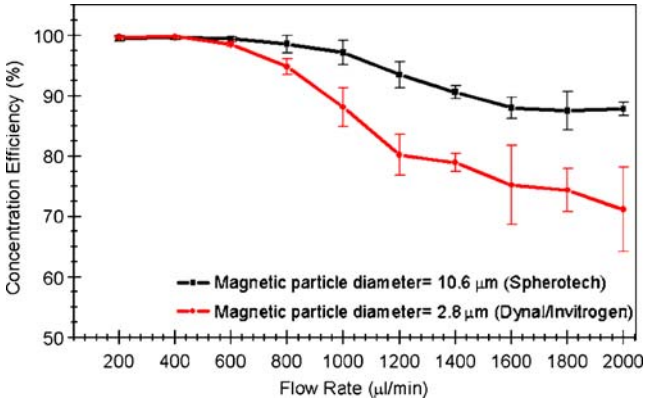

Fig. 6 Concentration efficiency versus flow rate

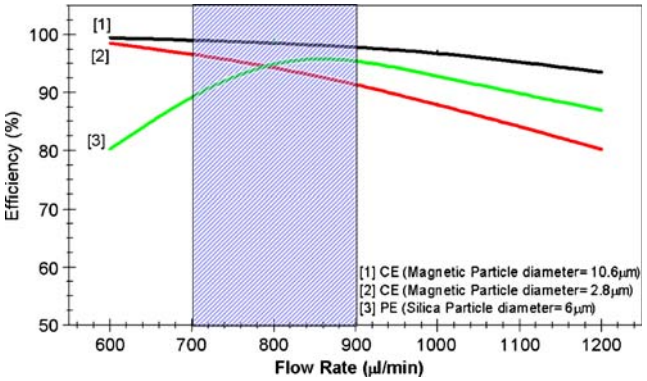

Fig. 8 The best results for concentration and purification can be achieved by setting the flow rate within the range 700–900 µl/min. *CE* concentration efficiency, *PE* purification efficiency

should be modified, e.g., by using larger magnets or increasing the magnetic field gradient by using magnetic flux concentrators at the trapping zones [17, 18]. Figure 7 shows the purification efficiency increases with increasing flow rate within the range from 400 to 900 µl/min, with the highest value of 99% at a flow rate of 800 µl/min, and decreased with higher flow rates. Both concentration and purification are crucial factors in any sample preparation system where capturing all the target analyte with maximum purity is the ultimate goal. From the results shown in Figs. 6 and 7, it can be concluded that the best results for concentration and purification with the MSS can be achieved by setting the flow rate within the range 700–900 µl/min (Fig. 8). In addition, the sample purity can be further enhanced by increasing the number of washing cycles through the MSS by increasing the number of magnets within the magnetic assembly under the fluidic channel as shown in Fig. 9.

The trapping and releasing event resembles one washing cycle in conventional biological assays. A direct application of the device is water-sample preparation for subsequent detection of waterborne pathogens in water quality monitoring laboratories.

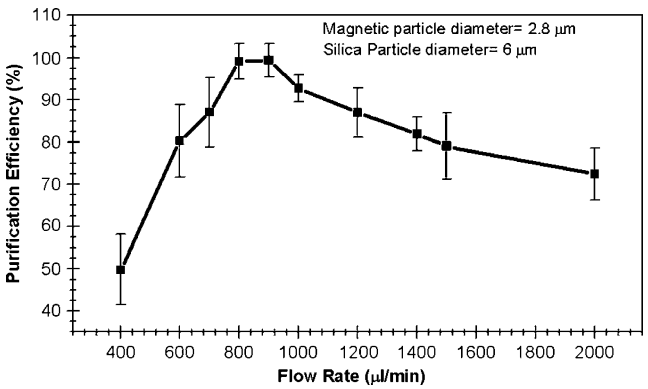

Fig. 7 Purification efficiency versus flow rate

Conclusions

An integrated system for sample preparation which is based on the concept of alternate trapping and releasing of particles under continuous-flow conditions has been designed, fabricated, and tested for applications dealing with very dilute samples. Each trapping and releasing event allows the surrounding buffer to wash the sample. The periodic washing events along the fluidic channel ensure a sample of high purity is collected at the end of the channel. Concentration efficiencies of 99.75±0.083% at a flow rate of 200 µl/min and 88.10±3.17% at a flow rate of 1,000 µl/min and a purification efficiency of 99.10±4.3% at a flow rate of 900 µl/min were achieved. In general, the method and the results obtained from this work demonstrate the feasibility of implementing sample purification in a closed-loop protocol that minimizes human interference, sample loss, and cross-contamination. This approach represents a step forward toward a fully automated sample preparation system for relatively large starting samples such as water.

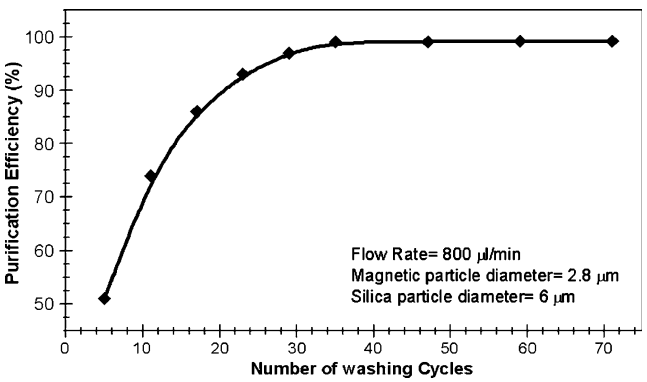

Fig. 9 The purification efficiency increases with increasing number of washing cycles through the MSS by increasing the number of magnets within the magnetic assembly under the fluidic channel

Acknowledgements This research was supported by A star-Exploit Technologies (ETPL) under Flagship grant no. F07/E/013. The authors thank ETPL and the Institute of Microelectronics for their support.

References

1. Gijs MAM (2004) Microfluid Nanofluid 1:22–40
2. Nicole P (2006) Lab Chip 6:24–38
3. Yavuz CT, Prakash A, Mayo JT, Colvin V (2009) Chem Eng Sci 64:2510–2521
4. Invitrogen (2008) Dynabeads® CD4. http://tools.invitrogen.com/content/sfs/manuals/111.45_Dynabeads%20CD4.(rev003).pdf
5. Carpino F, Moore LR, Zborowski M, Chalmers J, Williams S (2005) J Magn Magn Mater 293:546–552
6. Augusto PA, Grande TC, Augusto P (2005) Chem Eng J 111:85–90
7. Rotariu O, Ogden ID, MacRae M, Udrea LE, Strachan NJC (2005) Phys Med Biol 50:2967–2977
8. Barbic M, Mock JJ, Gray AP, Schultz S (2001) Appl Phys Lett 79:1399–1401
9. Inglis D, Riehn R, Austin RH (2004) Appl Phys Lett 85:5093–5095
10. Lee H, Purdon AM, Westervelt RM (2004) Appl Phys Lett 85:1063–1065
11. Ramadan Q, Samper V, Poenar DP, Chen Y (2006) J Micro-electromech Syst 15:624–638
12. Sinha A, Ganguly R, Puri K (2009) J Magn Magn Mater 321:2251–2256
13. Rida A, Fernandez V, Gijs MAM (2003) Appl Phys Lett 83:2396–2398
14. Ramadan Q, Samper V, Chen Y, Poenar DP (2006) Appl Phys Lett 88:032501–032503
15. Hatch GP, Stelter RE (2001) J Magn Magn Mater 225:262–276
16. Zborowski M, Chalmers JJ, Williams PS (2005) In: Cazes J (ed) Encyclopedia of chromatography. CRC, Boca Raton
17. Deng T, Prentiss M, Whitesides GM (2002) Appl Phys Lett 80:461–463
18. Ritter JA, Ebner AD, Daniel KD, Stewart KL (2004) J Magn Magn Mater 280:184–201